Relationship between Core Size, Side Chain Length, and the Supramolecular Organization of Polycyclic Aromatic Hydrocarbons

Wojciech Pisula, Željko Tomović, Christopher Simpson, Marcel Kastler, Tadeusz Pakula, and Klaus Müllen*

Max-Planck-Institute for Polymer Research, Ackermannweg 10, D-55128 Mainz, Germany

Received February 2, 2005. Revised Manuscript Received May 23, 2005

The effects of the core size, the side chain length, and the number of substituents on the supramolecular organization of polycyclic aromatic hydrocarbons have been investigated by 2D wide-angle X-ray scattering experiments performed on oriented filaments prepared by extrusion. The aromatic core size of the compounds varied between the hexa-*peri*-hexabenzocoronene core consisting of 42 carbon atoms and the enlarged aromatic core of 132 carbon atoms, whereas the length of the side chains extended up to 20 carbon atoms per chain. It has been observed that the lateral packing characterized by the lattice constant of the 2D intercolumnar hexagonal arrangement increases with the molecular masses of the core, forming the columnar stacks, and of the side chains which fill the core periphery. A model describing the relationship between the morphological and molecular parameters for the columnar hexagonal arrangements of the discotics is suggested and indeed proven by comparison with the experimental results.

Introduction

Since liquid crystalline discotic materials with large aromatic cores were successfully implemented in electronic devices such as photovoltaic cells and field-effect transistors,[1−3] the research interest in this kind of materials increased significantly within recent years. The discotic molecules self-organize by π stacking into columnar supramolecular structures facilitating a charge carrier transport along these 1D assemblies.[4−6] The intracolumnar charge carrier mobility is one of the most important factors in the design of electronic devices based on organic materials. It is, however, not yet clear which supramolecular parameters can lead to applicable results. Van de Craats and Warman have revealed a dependence of the intrinsic charge carrier mobility on the size of the aromatic core in the hexagonal liquid crystalline phase.[7] On the other hand, recent studies have suggested that this dependence works only up to the core size of hexa-*peri*-hexabenzocoronene (HBC) possessing the highest charge carrier mobility of 1.0 cm^2/Vs.[8] This shows that, besides the cofacial packing area of the discotic cores and the resulting $\pi-\sigma$ attractions of adjacent molecules,[9] there are other structural parameters relevant for the charge carrier mobility. Therefore, both the development of new alignment techniques[2,10−16] and a control of the supramolecular organization by tuning the architecture of single molecules as building blocks still constitutes a challenge in device fabrication.

The thermotropic phases of the HBC derivatives and other polycyclic aromatic hydrocarbons (PAHs) have already been extensively investigated using differential scanning calorimetry (DSC) measurements indicating the transition temperatures, X-ray diffraction revealing the supramolecular arrangements, and solid-state NMR providing information about the dynamics of the molecules.[17−22] In the crystalline state, the HBC disks revealed a reduced dynamics of the

* Corresponding author. Tel: (+49) 6131 379 150. Fax: (+49) 6131 379 350. Email: muellen@mpip-mainz.mpg.de.

(1) Schmidt-Mende, L.; Fechtenkötter, A.; Müllen, K.; Moons, E.; Friend, R. H.; MacKenzie, J. D. *Science* **2001**, *293*, 1119.
(2) van de Craats, A. M.; Stutzmann, N.; Bunk, O.; Nielsen, M. M.; Watson, M.; Müllen, K.; Chanzy, H. D.; Sirringhaus, H.; Friend, R. H. *Adv. Mater.* **2003**, *15*, 495.
(3) Pisula, W.; Menon, A.; Stepputat, M.; Lieberwirth, I.; Kolb, U.; Tracz, A.; Sirringhaus, H.; Pakula, T.; Müllen, K. *Adv. Mater.* **2005**, *17*, 684.
(4) Adam, D.; Schuhmacher, P.; Simmerer, J.; Haussling, L.; Siemensmeyer, K.; Etzbach, K. H.; Ringsdorf, H.; Haarer, D. *Nature* **1994**, *371*, 141.
(5) Boden, N.; Bushby, R. J.; Clements, J.; Jesudason, M. V.; Knowles, P. F.; Williams, G. *Chem. Phys. Lett.* **1988**, *152*, 94.
(6) Boden, N.; Bushby, R. J.; Clements, J.; Movaghar, B.; Donovan, K. J.; Kreouzis, T. *Phys. Rev. B* **1995**, *52*, 13274.
(7) van de Craats, A. M.; Warman, J. M. *Adv. Mater.* **2001**, *13*, 130.
(8) Debije, M. G.; Piris, J.; de Haas, M. P.; Warman, J. M.; Tomovic, Z.; Simpson, C. D.; Watson, M. D.; Müllen, K. *J. Am. Chem. Soc.* **2004**, *126*, 4641.
(9) Hunter, C. A.; Sanders, J. K. M. *J. Am. Chem. Soc.* **1990**, *112*, 5525.
(10) Tracz, A.; Jeszka, J. K.; Watson, M. D.; Pisula, W.; Müllen, K.; Pakula, T. *J. Am. Chem. Soc.* **2003**, *125*, 1682.
(11) Piris, J.; Debije, M. G.; Stutzmann, N.; Laursen, B. W.; Pisula, W.; Watson, M. D.; Bjørnholm, T.; Müllen, K.; Warman, J. M. *Adv. Funct. Mater.* **2004**, *14*, 1053.
(12) Piris, J.; Pisula, W.; Tracz, A.; Pakula, T.; Müllen, K.; Warman, J. M. *Liq. Cryst.* **2004**, *31*, 993.
(13) Piris, J.; Pisula, W.; Warman, J. M. *Synth. Met.* **2004**, *147*, 85.
(14) Pisula, W.; Tomovic, Z.; Stepputat, M.; Kolb, U.; Pakula, T.; Müllen, K. *Chem. Mater.* **2005**, *17*, 2641.
(15) Pisula, W.; Kastler, M.; Wasserfallen, D.; Pakula, T.; Müllen, K. *J. Am. Chem. Soc.* **2004**, *126*, 8074.
(16) Laursen, B. W.; Norgaard, K.; Reitzel, N.; Simonsen, J. B.; Nielsen, C. B.; Als-Nielsen, J.; Bjornholm, T.; Solling, T. I.; Nielsen, M. M.; Bunk, O.; Kjaer, K.; Tchebotareva, N.; Watson, M. D.; Müllen, K.; Piris, J. *Langmuir* **2004**, *20*, 4139.
(17) Fischbach, I.; Pakula, T.; Minkin, P.; Fechtenkötter, A.; Müllen, K.; Spiess, H. W.; Saalwachter, K. *J. Phys. Chem. B* **2002**, *106*, 6408.
(18) Tchebotareva, N.; Yin, X. M.; Watson, M. D.; Samori, P.; Rabe, J. P.; Müllen, K. *J. Am. Chem. Soc.* **2003**, *125*, 9734.
(19) Fischbach, I.; Ebert, F.; Spiess, H. W.; Schnell, I. *Chemphyschem* **2004**, *5*, 895.
(20) Wu, J. S.; Watson, M. D.; Zhang, L.; Wang, Z. H.; Müllen, K. *J. Am. Chem. Soc.* **2004**, *126*, 177.
(21) Fechtenkötter, A.; Saalwachter, K.; Harbison, M. A.; Müllen, K.; Spiess, H. W. *Angew. Chem., Int. Ed. Engl.* **1999**, *38*, 3039.

10.1021/cm050251c CCC: $30.25
Published on Web 07/20/2005

aromatic core, whereby most of the compounds also showed a molecular tilting with respect to the columnar axis. While the π interaction of the aromatic cores leads to self-assembly into the columnar structures, the side chains are partially organized in the core periphery usually with intercalation of chains of adjacent cores. The intercolumnar arrangement can be represented by means of a 2D lateral unit cell. At the transition temperature from the crystalline state to the liquid crystalline phase both the intra- and intercolumnar organization undergo considerable changes. During heating to the liquid crystalline phase, the molecular arrangement changes from a herringbone order to an orthogonal intracolumnar packing of the disks with respect to the columnar axis. Because of the cylindrical columnar symmetry, the hexagonal organization is favored being the most frequent lattice type observed in this phase. Furthermore, longitudinal and lateral displacements of the molecules occur within the stacks due to a high side chain mobility and the increase of their steric requirements at the high temperature phases. Additionally, molecular rotation around the column axes takes place. Because of this high degree of core mobility, intracolumnar disorder and nematic columnar phases can appear. The isotropization temperature depends strongly on the steric interaction of the side chains and their influence on the aromatic core interaction.[23] The steric demand can be significantly increased by introduction of long, branched side chains possessing large space-filling properties in the close vicinity of the corona.[15,24] Thereby, the isotropization temperature can be lowered from 420 °C for an *n*-alkylated HBC derivative to even room temperature for a dove-tailed HBC compound. In the isotropic state the discotic molecules are not isolated but form small aggregates consisting of 3−6 molecules.[24]

In general, little is known about the relation between the molecular architecture of the single building block and the resulting supramolecular structure. Desiraju and Gavezzotti have investigated the energetic and geometrical criteria for four basic crystal structure types of PAHs.[25,26] They observed that the type of adopted structure depends on the relative importance of the interaction between carbon−carbon and carbon−hydrogen interaction and therefore on the number and intramolecular positioning of these atoms. In this work, results of a comparative study of the molecular packing depending on the core size and the side chain length are presented. The intra- and intercolumnar packing parameters of the different discotic systems are compared in their hexagonal columnar phases and are described additionally by a simple model.

Experimental Section

A broad spectrum of discotic compounds is investigated in this study. The core size is varied from the HBC core consisting of 42 carbon atoms up to a large aromatic core of 132 carbon atoms. Since the IUPAC nomenclature is not trivial for these kind of structures, the aromatic cores and side chains are assigned by using simply the number of carbon atoms. The core structures are shown in Figure 1, and the side group types are presented in Figure 2. The longest alkyl side chain consisted of 20 carbons, whereas plain HBC and C96 cores were also studied. Not all possible combinations of cores and side chains have been realized. Nevertheless, the large number of materials studied, as listed in Table 1, covers a broad variety of possible architectures and the related range of volume fractions of the constituents. The synthesis of the HBC derivatives, C60, C78, C78−Star, C96, and C132, was described elsewhere.[22,27−31] Because of the increase of π conjugation, the color

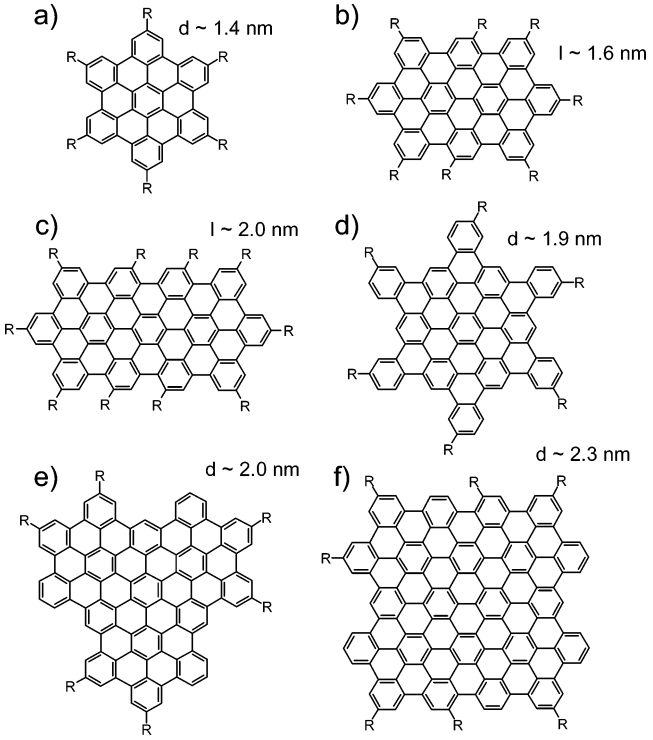

Figure 1. Chemical structures of the investigated PAHs with different core sizes: (a) HBC (C42), (b) C60, (c) C78, (d) C78−Star, (e) C96, and (f) C132.

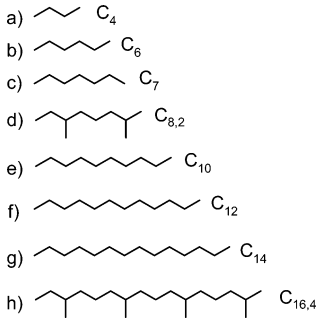

Figure 2. Structures of different side chains used in this study. The alkyl chains are described by the number of carbon atoms. The branched chains are labeled in a separate way.

(22) Herwig, P.; Kayser, C. W.; Müllen, K.; Spiess, H. W. *Adv. Mater.* **1996**, *8*, 510.
(23) Kastler, M.; Pisula, W.; Wasserfallen, D.; Pakula, T.; Müllen, K. *J. Am. Chem. Soc.* **2005**, 127, 4286.
(24) Pisula, W.; Tomovic, Z.; El Hamaoui, B.; Watson, M. D.; Pakula, T.; Müllen, K. *Adv. Funct. Mater.* **2005**, *15*, 893.
(25) Desiraju, G. R.; Gavezzotti, A. *Acta Crystallogr. B* **1989**, *45*, 473.
(26) Desiraju, G. R.; Gavezzotti, A. *Acta Crystallogr. B* **1988**, *44*, 427.
(27) Stabel, A.; Herwig, P.; Müllen, K.; Rabe, J. P. *Angew. Chem., Int. Ed. Engl.* **1995**, *34*, 1609.
(28) Liu, C. Y.; Fechtenkötter, A.; Watson, M. D.; Müllen, K.; Bard, A. J. *Chem. Mater.* **2003**, *15*, 124.
(29) Tomovic, Z.; Watson, M. D.; Müllen, K. *Angew. Chem., Int. Ed.* **2004**, *43*, 755.
(30) Iyer, V. S.; Yoshimura, K.; Enkelmann, V.; Epsch, R.; Rabe, J. P.; Müllen, K. *Angew. Chem., Int. Ed. Engl.* **1998**, *37*, 2696.
(31) Simpson, C. D. Dissertation, Johannes Gutenberg Universität, 2004.

Table 1. Basic Parameters of the Studied Discotics

sample	C core	C side	f[a]	transition temperatures (°C)[b]	a_{hex} (nm)	d (nm)
HBC	42	0	6	not observed	1.28	0.342
HBC−$(C_4)_6$	42	4	6	not observed	1.85	0.347
HBC−$(C_6)_6$	42	6	6	not observed	2.20	0.353
HBC−$(C_{8,2})_6$	42	10	6	(Cr) 81 (Col_h) ∼ 420 (I)	2.64	0.361
HBC−$(C_{10})_6$	42	10	6	(Cr) 124 (Col_{ho}) ∼420 (I)	2.63	0.362
HBC−$(C_{12})_6$	42	12	6	(Cr) 107 (Col_{ho}) ∼420 (I)	2.83	0.363
HBC−$(C_{14})_6$	42	14	6	(Cr) 114 (Col_{ho}) ∼420 (I)	3.02	0.360
HBC−$(C_{16,4})_6$	42	20	6	(Col_p) -36 (Col_{ho}) 231 (I)	3.37	0.370
HBC−$(C_{12})_4$	42	12	4	(Col_p) 146 (Col_{ho})	2.52	0.354
C60−$(C_{8,2})_8$	60	10	8	(Cr) 109 (Col_{ho})	2.74	0.372
C60−$(C_{12})_8$	60	12	8	(Cr) 104 (Col_{ho}) >450 (I)	3.13	0.376
C78−$(C_{12})_{10}$	78	12	10	(Cr) 87 (Col_{ho}) >450 (I)	3.25	0.394
C78−Star−$(C_{16,4})_6$	78	20	6	not observed	3.78	0.342
C96	96	0	6	not observed	2.0	0.343
C96−$(C_7)_6$	96	7	6	not observed	2.75	0.346
C96−$(C_{8,2})_6$	96	10	6	not observed	3.09	0.344
C96−$(C_{12})_6$	96	12	6	38 (no change in structure)	3.35	0.343
C96−$(C_{16,4})_6$	96	20	6	not observed	3.91	0.344
C96−$(C_{12})_4$	96	12	4	not observed	3.47	0.347/0.462[c]
C96−$(C_{14,10})_6$	96	24	6	not observed	3.47	0.36/0.471[c]
C132−$(C_{8,2})_8$	132	10	8	not observed	3.32	0.351
C132−$(C_{16,4})_8$	132	20	8	not observed	4.19	0.354

[a] f is the number of substituents. [b] Cr, crystalline phase; Col_p, plastic phase; Col_{ho}, hexagonal ordered mesophase; f, number of substituents. [c] d (tilted)/ period along the column.

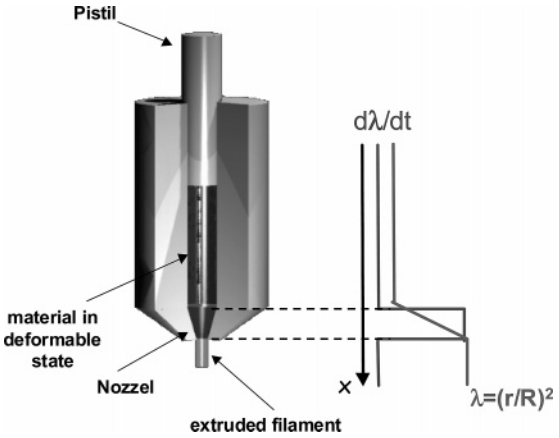

Figure 3. Schematic illustration of the filament alignment by extrusion using a mini extruder. Profiles of the drawing rate and the draw ratio along the extruder axis are schematically plotted on the right-hand side.

of the compounds is shifted from yellow (HBC) over orange and red to purple (C132).

The samples were prepared by filament extrusion using a home-built mini extruder which is presented schematically in Figure 3. Therein, the material is heated to a phase at which it becomes plastically deformable and is extruded as a thin filament by a constant-rate motion of the piston along the cylinder. This mechanical processing is controlled by a number of parameters: the velocity of the piston, diameters of cylinder and orifice, and the die shape. The ratio of the cylinder to orifice diameters defines the macroscopic draw ratio ($\lambda = (R/r)^2$) and the shape of the die defines the drawing rate profile. In the case of the conical die, as in the example shown in Figure 3, the drawing rate is constant within the die and is zero within the cylinder and at the die orifice. In the extruder used, the cylinder had an inner diameter of 2.0 mm and the orifice diameter was 0.7 mm. In this way, 0.7 mm thick filaments drawn to nearly $\lambda = 8$ were obtained. The piston has been moved typically with the rate of 5 mm/s which resulted in a high drawing rate within the die ($d\lambda/dt = 20$/s.). The X-ray diffraction experiments revealed that under such conditions the columns are in all cases well oriented in the direction of the extrusion. No effect of drawing rate on the structure could be detected.

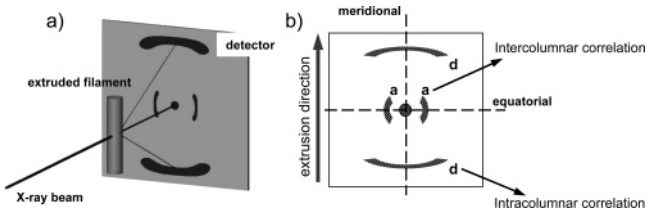

Figure 4. (a) Schematic representation of the experimental setup and (b) scheme of the characteristic 2D WAXS pattern of an extruded filament based on discotic molecules.

The structure investigation was performed using a 2D wide-angle X-ray scattering (WAXS) setup, which is shown schematically in Figure 4. The sample was positioned perpendicular to the incident X-ray beam. From the reflection positions in the 2D WAXS pattern, it is possible to obtain information about the intra- and intercolumnar supramolecular organization. Since the fibers are placed vertically with respect to the incident X-ray beam, the meridional reflections correspond to the correlations resulting from disk stacking and the equatorial reflections distribution provide information about the intercolumnar order.

Results and Discussion

Figure 5 presents examples of 2D WAXS patterns characteristic for the mesophase of discotics consisting of different core sizes and different substituents. The distinct meridional and equatorial reflections indicate a pronounced order within the extruded filaments. The meridional reflections corresponding to the intracolumnar correlations resulting from the π stacking of the molecules imply the arrangement of the disks orthogonal to the columnar axis in all analyzed cases. Since aromatic cores form the columnar stacks by π-stacking interaction and the side chains are disordered in the periphery, the equatorial reflection distribution can be fitted to a lateral 2D unit cell which characterizes the intercolumnar organization due to the correlation between aromatic cores in different columns. The characteristic 2D hexagonal lattice was assigned for all systems being in the mesophase. In most cases, such a structure was indicated by the typical peak positions of $1:\sqrt{3}:2:\sqrt{7}$, whereby the

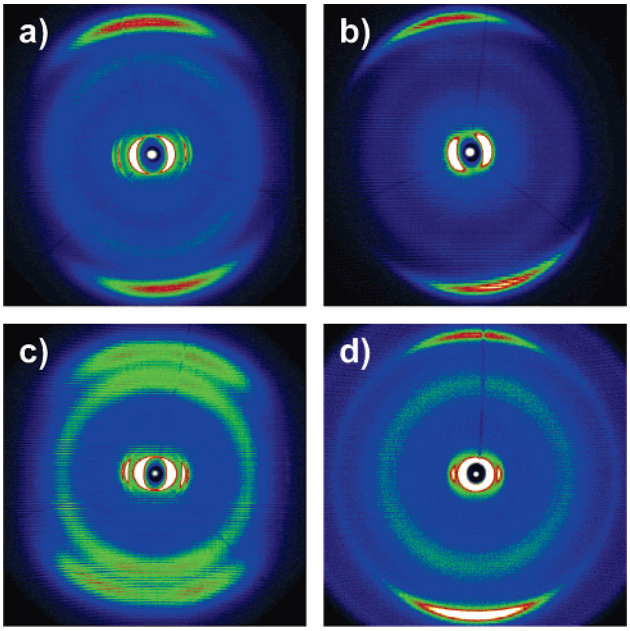

Figure 5. Characteristic 2D WAXS patterns of (a) HBC−$(C_{10})_6$, (b) C96−$(C_7)_6$, (c) C60-$(C_{12})_8$, and (d) C78−Star−$(C_{16,4})_6$. All compounds are in the mesophase.

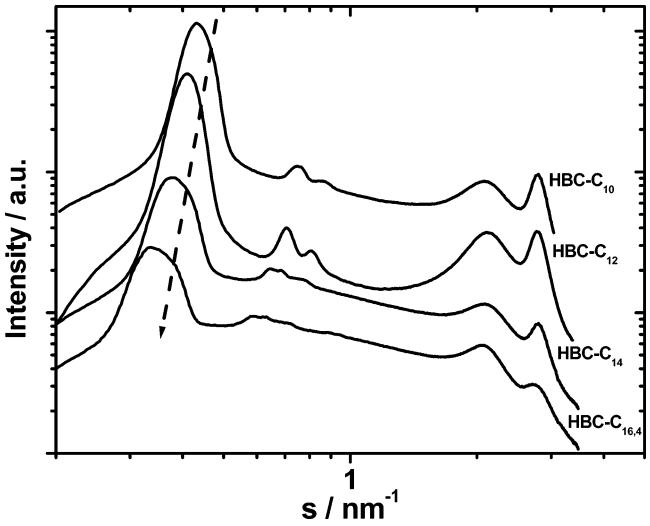

Figure 6. Scattering intensity distributions as a function of the scattering vector for HBC derivatives substituted by side chains of different length.

proportions of intensities at various positions were system dependent. An explanation of this effect is briefly discussed in the Appendix where the scattering effects from the hexagonal columnar arrangement are considered as being dependent on the core size and the volume fraction of the side chain phase i.e., the parameters which have been varied in a broad range in the studied samples. It is pointed out in the Appendix that a disappearance or weakness of higher order reflections must not necessarily be correlated with the range and degree of the columnar order but can also result from specific volume ratios between aromatic columns and the peripheral side chains.

The effects of the variation of the architectural parameters, such as the side chain length and the aromatic core size, of the discotic molecules on the scattering intensity distributions are illustrated in Figures 6 and 7. As an example, the scattered intensity distributions, averaged over the azimuthal angle, shown in Figure 6 illustrate impressively the relation

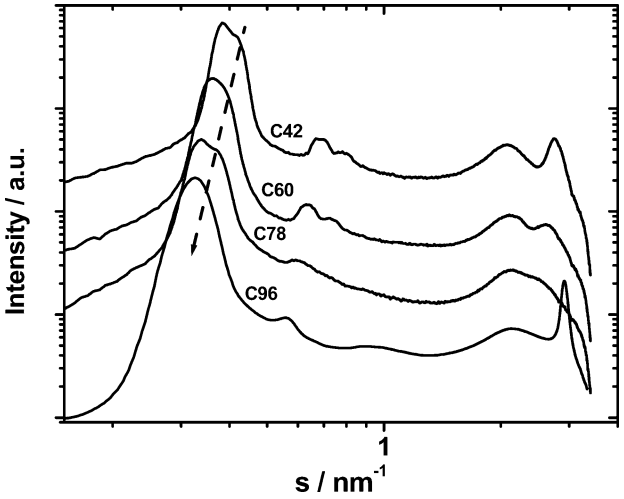

Figure 7. Scattering intensity distribution as a function of the scattering vector for different discotic molecules each substituted by C_{12} alkyl chains.

between the side chain length and the parameters of the lateral packing of columns for different 6-fold substituted HBC derivatives. The intensity distributions are plotted as a function of the scattering vector s (defined as $s = 2 \sin \theta/\lambda$, where 2θ is the scattering angle). The results show a shift of the reflections to lower s values with increasing side chain length. This shift can be correlated to increasing unit cell parameters which expand from 2.69 nm determined for HBC−$(C_{10})_6$ to 3.37 nm found for HBC−$(C_{16,4})_6$.

While the lateral organization of columns is strongly dependent on the substituents, the intracolumnar period in the mesophase remains in the typical range between 0.34 and 0.37 nm for the investigated HBC derivatives, whereby the value increases slightly with increasing side chains length. This difference of the intracolumnar dimensions can be correlated with the increase of the steric requirements of longer side chains, which hinder a closer approach of the aromatic cores. Additionally, a characteristic amorphous halo was observed for each HBC compound at a correlation distance of 0.46 nm.

The X-ray diffractogram in Figure 7 reveals effects of core size on the unit cell parameters describing the columnar packing. The structures of discotic molecules with different core sizes, but each substituted by C_{12} alkyl chains, are taken into account here. It has been found that the intercolumnar distance increases with increasing core size as indicated by the shift of the reflections to smaller scattering values. The aromatic core size of the compounds shown in Figure 7 varies from HBC with a diameter of approximately 1.4 nm to the C96 core with a size of about 2.0 nm. This difference in core size is also reflected in the different hexagonal unit cell parameters obtained for these compounds which were $a =$ 2.83 nm for HBC−$(C_{12})_6$ and $a = 3.35$ nm for C96−$(C_{12})_6$. It should be noted that the cores C42, C78−Star, and C96 were 6-fold substituted by the C_{12} alkyl chains, whereas eight side chains were attached to the C60 core. Nevertheless, the trend of the increasing unit cell dimensions with larger core size is obvious. Furthermore, it can be supposed that the symmetric shape of the core is not essential since the molecules perform a lateral rotation due to their high mobility in the mesophase resulting in an average effective core geometry.[17]

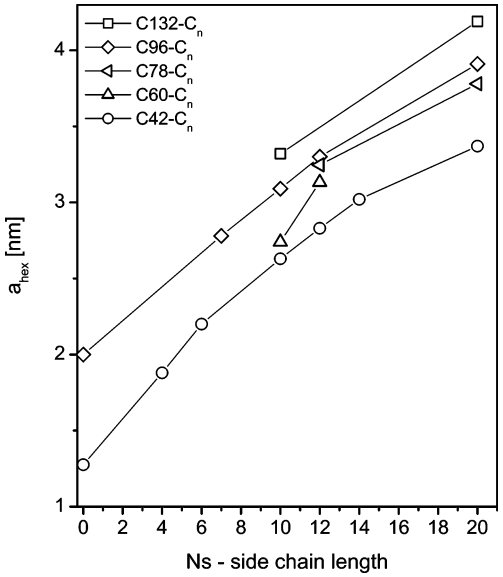

Figure 8. Hexagonal unit cell dimensions as a function of the side chain length for various core sizes. The lines are eye guides connecting points characterizing systems with the same core size.

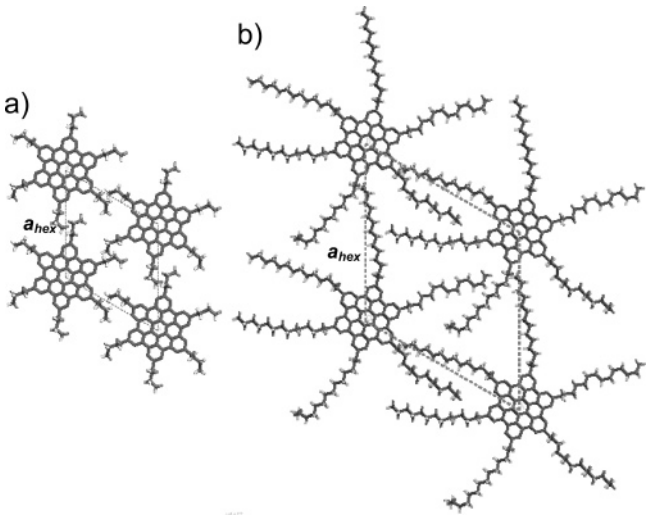

Figure 9. Examples of two hexagonal lattice arrangements consisting of (a) HBC−$(C_4)_6$ and (b) HBC−$(C_{14})_6$.

In Figure 8, the hexagonal intercolumnar spacings for all the investigated compounds are summarized as a function of the side chain length for various core sizes. A similar dependence of the lattice parameters on the side chain length is observed for the HBC and C96 cores. Both dependencies reveal the same trend, whereas all the C96 packing parameters are shifted by ca. 0.6 nm to higher distances due to the larger core disk. Both curve shapes are not linear and seem to level off for longer substituents. This behavior provides a strong indication that the side chains in the mesophase realign into a continuous intercolumnar phase filling the space between the columns, whereby the degree of interdigitation of the side chains can be considered to increase for longer chains. Similar packing behavior has been reported for triphenylene derivatives.[32] In Figure 9, the intercolumnar hexagonal arrangement is illustrated for two HBC derivatives

(32) Allen, M. T.; Harris, K. D. M.; Kariuki, B. M.; Kumari, N.; Preece, J. A.; Diele, S.; Lose, D.; Hegmann, T.; Tschierske, C. *Liq. Cryst.* **2000**, *27*, 689.

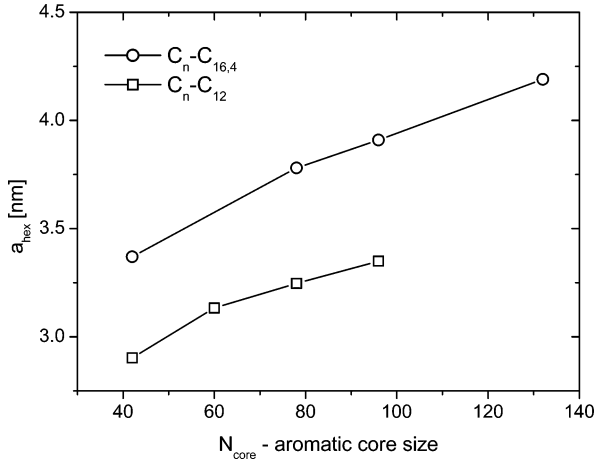

Figure 10. Hexagonal unit cell parameters as a function of the core size for two side chain lengths. The lines are eye guides connecting points characterizing systems with the same side chain size.

substituted by short and long alkyl side chains taken as examples.

The dependence between the core size and the 2D unit cell parameters of the columnar packing is presented in Figure 10 for two lengths of the side chains. The aromatic core mass is expressed by the number of carbon atoms and the intercolumnar packing lattice parameters for disks substituted by the linear C_{12} alkyl chains and the branched $C_{16,4}$ chains are given. All the results presented indicate that the morphological parameters of the studied systems are related to the packing possibilities in the two phases: the aromatic columnar cores and the aliphatic chains constituting the periphery. The disk cores forming the columns in all systems remain at distances between 0.34 and 0.36 nm, which are only slightly higher than the interlayer distances of graphite (0.34 nm). This suggests that the density of the columns is nearly that of the graphite ($\rho_c = 2.25$ g/cm^3). Such packing within the columns has to be in balance with the packing of the aliphatic side chains filling the space between them. By assumption of the density $\rho_s = 0.9$ g/cm^3 (corresponding nearly to amorphous wax) for the side chain phase, the intercolumnar distances can be related to the spatial requirements of the side chains given by their length and number. This can be expressed by the following relation based on the geometry illustrated in Figure 9

$$\frac{a_{hex}^2 d\_3}{2} = V_{core} + V_{sc} \quad (1)$$

where V_{core} and V_{sc} are volume fractions of the core and the side chain phases per repeating distance d along the column, respectively. By consideration of relations between these volume fractions and the molecular weights of the corresponding molecular moieties, the intercolumnar distance a_{hex} can be given by the following relation

$$a_{hex} = \sqrt{\frac{2}{dN_A\_3}\left(\frac{M_c}{\rho_c} + \frac{fM_s}{\rho_s}\right)} \quad (2)$$

where N_A is the Avogadro number, M_c and M_s are molecular masses of the core and a single side chain, respectively, and f is the number of side chains in the discotic molecule. This

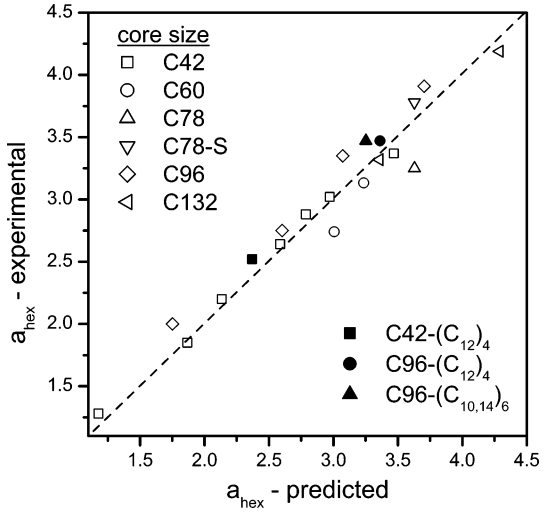

Figure 11. Comparison of the predicted and experimental values of the hexagonal lattice constants for columnar bulk structures. The dashed line indicates the predicated values. Each type of aromatic core is represented by one symbol, which indicates for the corresponding disk size all lattice parameters determined dependent on the length of the side chains.

relation allows predictions concerning intercolumnar distances in the hexagonal arrangement when the molecular parameters (M_c, M_s, and f) are known. The values predicted for the hexagonal lattice constants are compared in Figure 11 with the values determined experimentally on the bases of the X-ray diffraction intensities. Thereby, it is obvious that eq 2describesvery well the packing conditions of the discotic molecules. Modifications of the assumed densities could further improve the correlation.

Since both the HBC 6-fold substituted by linear C_{10} alkyl chains and the HBC substituted by branched $C_{8,2}$ side chains reveal the same lattice parameters, it is assumed that the packing possibilities related to the number of carbon atoms within the side chains has a larger influence on the intercolumnar organization than the details of the chemical architecture. However, this statement is not valid generally. An exception has been observed for longer dove-tailed side chains with very different mass distribution in the side groups. Branching of side chains close to the discotic core can result in a high steric demand and increase chain interactions in the disk periphery which are too large to allow the orthogonal arrangement of disks in the columns preserving the characteristics for strong π stacking distances. Such constraints can, however, relax through a tilt of disks with respect to the columnar axes in the mesophase, which in effect leads to an extension of columns and increase of the space around them.

The number of alkyl chains attached to the aromatic core can also influence the intercolumnar packing. The supramolecular organization of some discotic cores with a reduced number of side chains, i.e., HBC$-(C_{12})_4$, C96$-(C_{12})_2$, C96$-(C_{12})_4$, and with dove-tailed side chains C96$-(C_{14,12})_6$, have, therefore, been investigated. Examples of the 2D WAXS patterns for the systems with different side chain numbers are shown in Figure 12. The sample C96$-(C_{12})_2$ was not processable by filament extrusion due to strong π stacking and the reduced degree of freedom of the side chains leading to insufficient plasticity of the material. The powder X-ray

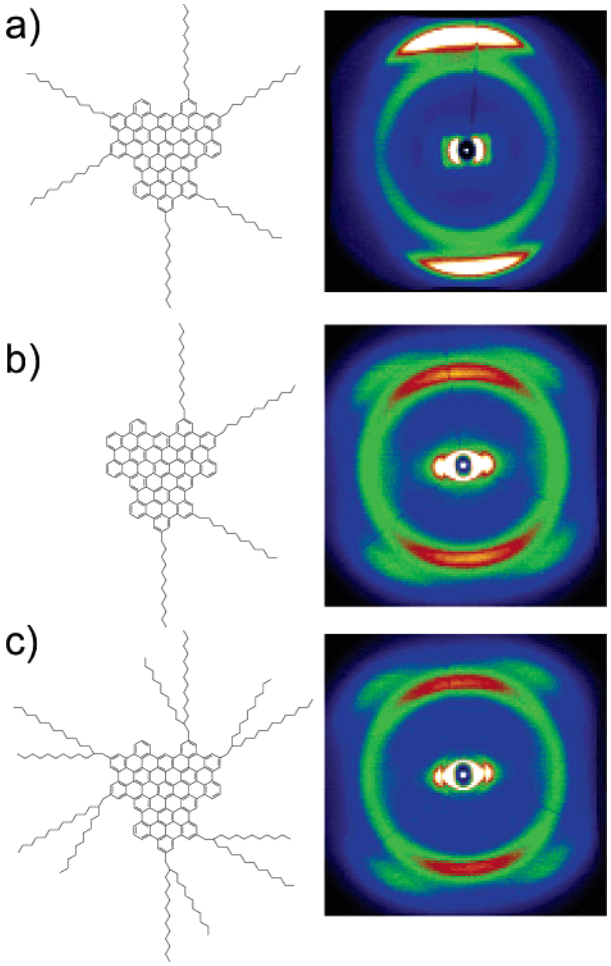

Figure 12. Structure investigation by using 2D WAXS experiments dependent on the number of side chains substituted to the C96 core with (a) C96$-(C_{12})_6$, (b) C96$-(C_{12})_4$, and (c) C96$-(C_{14,12})_6$.

diffraction of this material revealed only one broad small angle peak at $s = 0.38$ nm^{-1} and therefore the lattice could not be assigned precisely. In the other cases, independent of the asymmetry of some molecules, the hexagonal 2D lattices were detected. In some cases, however, a tilting of disks with respect to the columnar axis was observed which resulted in increased periods along the columns. The lattice constants of the intercolumnar packing in such systems are also considered in the comparison between experimental and predicted values presented in Figure 11. For the system HBC$-(C_{12})_4$ in which the typical orthogonal disk orientation with respect to the column axes was detected for the mesophase (Figure 13b), the comparison reveals a good agreement. In the crystalline state the disk adopted the characteristic tilted intracolumnar arrangement (Figure 13c). Contrary to that, in the system C96$-(C_{12})_4$, the tilt of disks was detected also in the mesophase and the hexagonal lattice constant was not satisfying the eq 2 when columns of cross-section corresponding single disks area were considered. The by far too large lattice constant observed experimentally can, however, be understood when columns built up of pairs of coplanar adjacent disks are considered. Such pairs with eight arms each constitute more symmetric elements and, when tilted, fit to a nearly cylindrical cross section of the columns, which fit better to the detected hexagonal symmetry of the columnar arrangement.

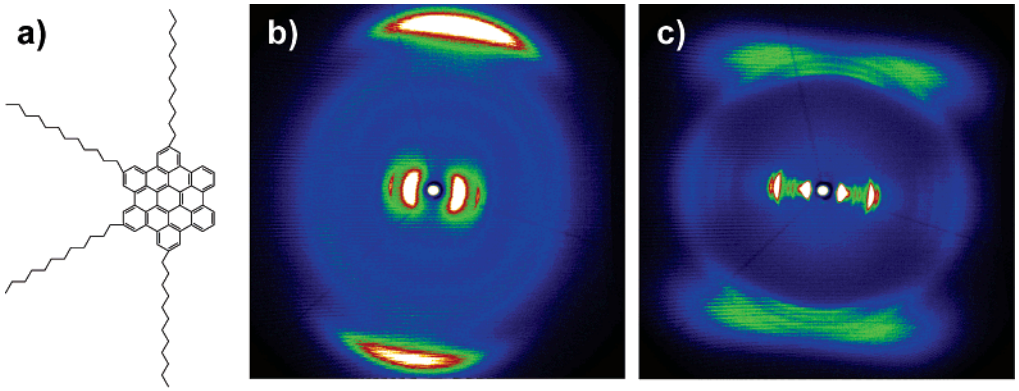

Figure 13. (a) Chemical structure of HBC−$(C_{12})_4$, 2D WAXS pattern of HBC−$(C_{12})_4$ in (b) the mesophase and (c) in the crystalline state after thermal treatment by annealing the extruded sample several times in the higher-temperature phase.

The other system with the detected tilt, C96−$(C_{14,12})_6$, is also in good agreement with eq 2 when the increased periodicity along the columns is considered. The tilt in this case has probably a different reason than in the other case. As discussed earlier in this paper, the crowd of side chains at the periphery of the disks requires column extension in order to be accommodated at the density characteristic for the side chain phase. This extension is realized by the tilt of disks with respect to the column axis. The observed agreement of the experimental and predicted lattice parameters for this system with the tilt taken into account strongly supports such a hypothesis.

The results presented indicate that the characteristic supramolecular structures and related parameters are controlled by packing possibilities of the stiff planar cores and the flexible side groups into separate phases of different densities. The balance of these packing possibilities with the π interactions in the columns should impose the structure stability and corresponding transition temperatures. In all the systems investigated, the structures reported extend over a very broad temperature range often exceeding the range of accessible temperatures because of chemical decomposition. This indicates that, for the studied molecular architectures, there is no conflict between packing possibilities and conditions for effectiveness of the π interactions. It can, however, be expected that in the systems with the tilt of disks, where the effectiveness of the π stacking is reduced at the expense of satisfaction of packing conditions, the stability of structures will become reduced as well.

Conclusions

In conclusion, the intercolumnar packing dimensions of the PAHs are strongly dependent on the aromatic core size, the side chain length, and the number of side chains. Influence of the different molecular parameters on the lattice constant of the hexagonal columnar morphology can be summarized in the relationship taking into account the two-phase packing with densities characteristic for each phase. A good agreement of the packing model with the experimental observations for the large variety of studied systems supports its predictive possibilities. This can be regarded as an example of consideration, which may play an important role in the improved design of molecules which are able to self-organize into tailored supramolecular structures.

Appendix

X-ray scattering is widely used to identify types of structures in liquid crystalline systems. In the case of columnar textures, 2D lattice types and parameters describing the lateral arrangement of column axes are derived.[17] Especially when the systems are oriented macroscopically, the reflections related to the columnar packing can be well separated from other correlation effects contributing to the scattering. In such cases, positions of the related (e.g., equatorial) scattered intensity peaks are compared with known sequences of Bragg reflections expected for various regular ordering schemes.[33] In this way, lamellar, hexagonal, rectangular, and monoclinic lattices can be distinguished. This works under the condition that the order is high enough and that it extends over sufficient distances to make observations of higher order scattering reflections possible. Weakly ordered structures usually cannot be resolved unambiguously because only the lower order and broad peaks appear in the scattering patterns. Using the X-ray scattering in such a way is the most popular method of identification of structures in the LC systems. Seldom more detailed analysis of the scattering is performed.[34] Essentially, for any structure, i.e., for the corresponding electron density distribution, the scattering intensities can be calculated by means of the simple Fourier transform of the assumed models. Such an approach allows not only a comparison of positions of peak sequences but also considerations of their intensities which may contain further information concerning details of the examined structure. A well-known example is the absence (zero intensity) of even order reflections in the lamellar systems indicating equal thickness of sublayers. Despite clear advantages of such a comparison, consideration of peak intensities has not been widely made especially for structures that are more complex than the lamellar one. We would like to demonstrate here some cases of hexagonal order in the studied systems for which the scattered intensity consideration can provide additional information and understanding concerning effects of volume fractions of the aromatic column cores with respect to the aliphatic matrix.

(33) Burger, C.; Zhou, S.; Chu, B. In *Handbook of Polyelectrolytes and Their Applications*; Tripathy, S. K., Kumar, J., Nalva, H. S., Eds.; American Scientific Publishers: 2002; Vol. 3, Chapter 7, p 125.
(34) Floudas, G.; Pispas, S.; Hadjichristidis, N.; Pakula, T. *Macromol. Chem. Phys.* **2001**, *202*, 1488.

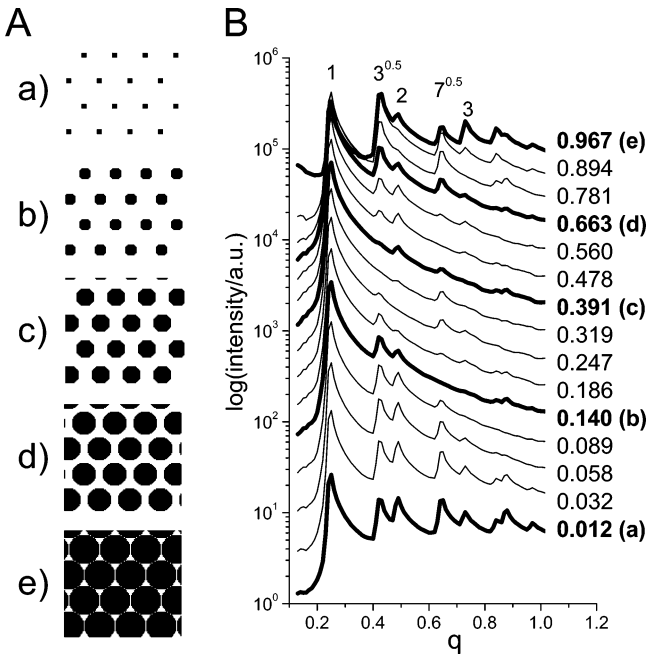

Figure 14. (A) Illustration of cross sections through hexagonal columnar structures with constant 2D lattice size but various volume fractions of the columnar phase, (B) predictions of scattered intensity distributions for hexagonal columnar structures with constant 2D lattice size but various volume fractions of the columnar phase. The cases assigned as a−e are related to respective structures shown in Figure A1.

Figure 14A shows examples of the 2D hexagonal structure of disks with various diameters for which an electron density contrast with respect to the matrix is assumed. The disk diameter variation under conditions of fixed lattice constants involves variation of the volume fractions of the two phases. Structure factors calculated for such systems with various compositions are shown in Figure 14B.

The structure factors have been determined by Fourier transformation of the 2D electron density patterns illustrated in Figure 14A. The perfect hexagonal order in the area consisting of 24 disks with varying sizes but at constant distances is assumed. Under such conditions, the peak positions of the structure factor remain constant but the intensities vary considerably with composition between the core and side chains. As indicted in Figure 14B, the positions of peaks satisfy the characteristic for hexagonal structure relations 1, $\sqrt{3}$, 2, $\sqrt{7}$, 3, etc.

The most characteristic cases are those in which intensities of some peaks are reduced to zero as in the above-mentioned symmetric lamellar AB system. In the case of the hexagonal lattice, there are several characteristic situations within the whole composition range:

- Structure factor maxima related to all characteristic diffraction lines are only well visible at small (less than 0.1) and large (more than 0.95, above 0.91 the disk phase becomes continuous) fractions of the discotic phase.
- Maxima related to diffraction lines at $\sqrt{3}$ and 2 nearly disappear at the composition 0.3; the next visible peak corresponds to the line $\sqrt{7}$, which might not be visible as well when the correlation extent is not large enough.
- In the composition range 0.3−0.45, the peak at $\sqrt{3}$ is not visible, whereas the maximum at 2 is distinguishable, such case can be mixed up with a lamellar structure.
- The maximum corresponding to the line at $\sqrt{3}$ becomes the most intensive when the discotic phase is approaching unity.
- The intensity peak corresponding to the line 2 disappears at two compositions ∼0.25 and ∼0.8−0.9.

Such and other atypical features of the structure factor for the hexagonal arrangement may considerably complicate an interpretation of experimental results when only positions of detectable intensity peaks are taken into account. As the present examples illustrate, knowledge about system composition might be of a considerable help in the assignment of more accurate unit cell structures.

Acknowledgment. This work was financially supported by the EU project NAIMO Integrated Project No NMP4-CT-2004-500355 and the Deutsche Forschungsgemeinschaft (Schwerpunktprogramm Organische Feldeffekttransistoren). M. Kastler thanks the Fonds der Chemischen Industrie and the Bundesministerium für Bildung und Forschung for financial support.

CM050251C